Single-ended DC Fault Location Method For MMC-Based HVDC Power System Using Adaptive Multi-step Levenberg-Marquardt Algorithm

Liu, Le; Xie, Fan; Popov, Marjan; Hao, Zhiguo; Lekic, Aleksandra

DOI
10.1109/PowerTech55446.2023.10202991

Publication date
2023

Document Version
Final published version

Published in
Proceedings of the 2023 IEEE Belgrade PowerTech

Single-ended DC Fault Location Method For MMC-Based HVDC Power System Using Adaptive Multi-step Levenberg-Marquardt Algorithm

Le Liu[1*], Fan Xie[1,2], Marjan Popov[1], Zhiguo Hao[2], and Aleksandra Lekić[1]
[1]*Faculty of Electrical Engineering, Mathematics & Computer Science, Delft University of Technology, Delft, The Netherlands*
[2]*School of Electrical Engineering, Xi'an Jiaotong University, Xi'an, China*
{L.Liu-7, F.Xie-1, M.Popov, A.Lekic}@tudelft.nl, zhghao@mail.xjtu.edu.cn

***Abstract*—This article presents an accurate DC fault location method that applies parameter fitting. This technique first discusses the traveling wave (TW) propagation process in the decoupled line-mode network. We obtain the exact fault distance equation based on the analytical expressions for the wavefront of backward line-mode voltage TW. The adaptive multi-step Levenberg- Marquardt's (AMLM) algorithm is used for parameter fitting due to its fast processing speed and accuracy. The exact fault location can then be estimated using the parameter fitting results. The proposed fault location method is validated using a three-terminal HVDC system modeled on a real-time digital simulator (RTDS) platform. Based on the experimental results, the proposed method accurately detects the fault location, with all estimated errors smaller than 1%, and can withstand 40 dB noise interference. Moreover, the proposed method does not need a high sampling frequency and communication device. Its accuracy is independent of fault resistance and type compared to existing methods.**

***Index Terms*—HVDC, VSC, backward traveling wave, DC fault location, parameter fitting, Levenberg-Marquardt, RTDS.**

I. Introduction

DUE to the merits of bulk power transmission capacity and flexible active/reactive power regulation, the modular multilevel converter (MMC)-based HVDC system is recognized as the preferred option for power transmission, integrating renewable generations and asynchronous power grids [1], [2]. Generally, HVDC transmission lines are long-distance lines passing along wicked corridors, which makes DC faults unpredictable. Thus, it is crucial to implement DC fault detection, fault clearance, fault location, and post-fault recovery schemes to maintain the stability of the HVDC system. An accurate fault location method would significantly reduce the fault impact and accelerate system restoration processes within these aspects.

Currently, substantive research has been conducted on DC transmission line fault location, including the natural frequency method, fault analysis method, active signal injection method, and traveling wave method. The natural frequency methods are proposed in [3]–[5]. These methods mainly rely on the characteristics of the natural frequency components presented in the post-fault voltage/current. Generally, these methods require an extremely high sampling frequency and fail to discriminate the fault location if the fault point is close to the line terminal. The fault analysis methods calculate the voltage/current expressions at any point and then locate the fault based on the fault characteristics of measured voltages/currents. The frequency analyzing methods in [6]–[9] do not require a high sampling frequency to identify the TW front. However, the accuracy of the fault analysis method is vulnerable to the transmission line parameters [10]. The fault location methods of active signal injection are proposed in [11]–[13], which actively inject a specific detecting signal and thus identify the fault location via the features of the response signals. However, additional equipment or a control loop for signal injection is required. Besides, the injected signal may also affect the stable operation of other healthy lines. The traveling-wave based-methods are featured high precision and reliability and are not influenced by fault resistance. The general principle is to establish the mathematical relationship between the TW's propagation time, velocity, and fault distance based on the TW's law. However, the performance of these methods have inherent drawbacks. For example, the double-ended methods in [14], [15] can only be applied in systems with accurate signal measurements and high-fidelity synchronized communication channels, which increase the overall investments and the risk of data damage during data synchronization. The single-ended methods in [16], [17] require an extremely high-sampling frequency to estimate the TW's precise velocity and are also susceptible to noise intervention.

According to the superposition theorem, the fault point can be seen as a Thévenin voltage source. The fault-induced voltage TW at the fault point is a step wave, which can be split up into backward and forward traveling waves. The wavefront of backward voltage traveling waves can be approximated as an exponential function, whose time constant is highly associated with fault distance [18]. To this end, the fault location can be realized by parameter fitting of the backward voltage TW's wavefront.

This study first analyzes the characteristics of the propagation process of backward line-mode voltage traveling wave (BLVTW). Then a novel on parameter fitting using the Adaptive Multi-step Levenberg-Marquardt (AMLM) algorithm for the fault location is proposed. Compared with the existing fault

2023 IEEE Belgrade PowerTech | 978-1-6654-8778-8/23/$31.00 ©2023 IEEE | DOI: 10.1109/POWERTECH55446.2023.10202991

location methods, the novelty and the main contributions of our research are threefold. Firstly, the proposed fault location method does not require an extremely high sampling frequency (20 kHz in this work) to detect the TW, significantly reducing hardware requirements and investment in practical applications. Secondly, the performance of the proposed method is not affected by fault resistance and fault type, which ensures its accuracy and robustness. Thirdly, the proposed method eliminates the need for additional communication and synchronization device precise estimation of TW velocity compared with traditional methods.

The rest of this paper is structured as follows. Section II gives the analytical expressions of backward line-mode voltage traveling waves. Section III demonstrates the proposed fault location method based on the AMLM algorithm. Section IV provides performance validation of the proposed fault location method via the RTDS platform. Finally, conclusions and future work are provided in Section V.

II. Characteristic of Backward Line-Mode Voltage Traveling Wave After DC Internal Fault

A. MMC-Based HVDC Power System Set-up

The structure of the studied system is given in Fig. 1. The voltage level is $\pm$525 kV, and thus, corresponds to the planned HVDC ratings in the North Sea. The control design for MMCs uses the principles outlined in Cigre B4.57 [19]. Specifically, MMC1 and MMC3 implement grid-following control to maintain the DC grid voltage and regulate the active power flow. The wind farms are configured to generate 2 GW of power and are connected to the system via MMC2 using grid-forming control.

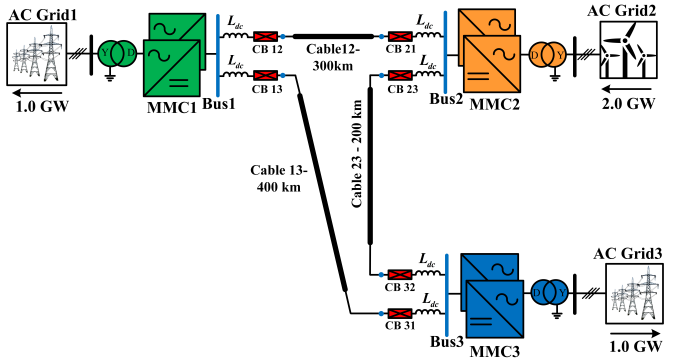

Fig. 1. Configuration of the studied system.

Each cable outlet features the relay units (marked as solid blue circles in Fig. 1) using the SIEMENS traveling wave protection (TWP) method, which is detailed in [20]. Additionally, each cable outlet employs the VSC-assisted resonant current (VARC) DCCB as described in [21]. The parameters of the VARC, originally presented in [21], have been scaled to fit the $\pm$525 kV system.

To accurately observe the propagation process of TW, the frequency-dependent (phase) cable model benchmarked by Cigre [19] is adopted. Cable12, cable23, and cable13 have lengths of 300 km, 200 km, and 400 km, respectively. The complete system parameters are shown in Table. I.

TABLE I
Parameters Of The MMC-based HVDC Power System

Parameter	MMC1	MMC2	MMC3
Nominal system frequency (Hz)	50	50	50
MMC (one pole) rated capacity (MVA)	1000	1000	1000
Transformer ratio (D/Y$_n$)	275/380	275/220	275/400
Transformer leakage inductance (p.u.)	0.18	0.18	0.18
Number of arm sub-module (SM)	200	200	200
Arm inductance (mH)	4.97	4.97	4.97
Capacitance of each SM (mF)	15	10	15
SM capacitor voltage rating (kV)	2.0	2.0	2.0
DC inductor L_{dc} (mH)	80	80	80

B. Initial Values of Voltage At The Fault Point

Through pole-mode transformation, the symmetrical bipolar transmission system can be represented as an independent line- and zero-mode network. The line- and zero-mode voltages v_1, and v_0, and currents i_1, and i_0 can be obtained by applying the following transformation matrix [22]:

$$\begin{bmatrix} v_0 \\ v_1 \end{bmatrix} = \frac{1}{\sqrt{2}} \begin{bmatrix} 1 & 1 \\ 1 & -1 \end{bmatrix} \begin{bmatrix} v_p \\ v_n \end{bmatrix}, \begin{bmatrix} i_0 \\ i_1 \end{bmatrix} = \frac{1}{\sqrt{2}} \begin{bmatrix} 1 & 1 \\ 1 & -1 \end{bmatrix} \begin{bmatrix} i_p \\ i_n \end{bmatrix}. \tag{1}$$

where v_p, v_n, i_p, and i_n denote the voltages and currents monitored at relays of positive and negative poles, respectively.

In contrast to zero-mode components (v_0, i_0), the line-mode components (v_1, i_1) propagate along polar lines and thus are not influenced by grounding. As a result, the loop parameters of line-mode components remain unchanged. Therefore, line-mode components are the preferred parameters in our work due to their higher propagation velocity and smaller attenuation constant.

The fault-induced initial values of the line-mode voltage at the fault point Δv_{F1} for a typical pole-to-pole fault (PTP), positive pole-to-ground (PTG) fault, and negative pole-to-ground (NTG) fault can be expressed as [23]:

$$\begin{cases} \Delta v_{F1} = \dfrac{-2\sqrt{2}U_f Z_{c(1)}}{2Z_{c(1)} + R_f}, & \text{(PTP)} \\ \Delta v_{F1} = \dfrac{-2U_f Z_{c(1)}}{Z_{c(1)} + Z_{c(0)} + 2R_f}, & \text{(PTG or NTG)} \end{cases} \tag{2}$$

where U_f refers to the rated DC voltage, R_f denotes the fault resistance, $Z_{c(1)}$ and $Z_{c(0)}$ represent the characteristic impedances in the line- and zero-mode network, respectively.

C. Expressions of BLVTW Measured At Internal Relay Unit

We assume that an internal fault f_{12} occurs at the studied faulty cable12. The TW propagation process in the line-mode network is illustrated in Fig. 2. The following contents in this subsection aim to achieve the analytical expressions of BLVTW measured relay units in cable 12.

In case of a fault, the voltage and current TWs propagate from the fault point to cable terminals and will be partly reflected and transmitted to the other grid sections when the

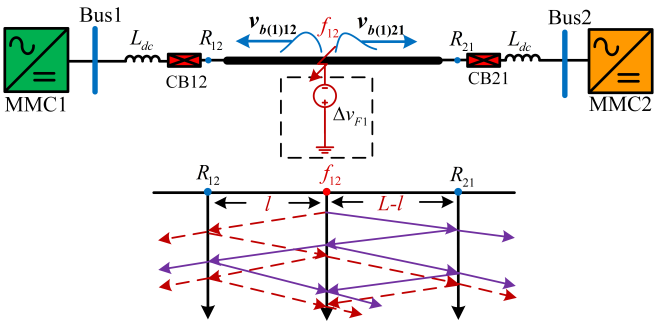

Fig. 2. Diagram of TW propagation process in faulty cable12.

wave impedance changes. According to the TW theory [23], the line-mode voltage $v_{(1)}(l,t)$ and the current $i_{(1)}(l,t)$ propagate with the time and space. The expressions for $v_{(1)}(l,t)$ and $i_{(1)}(l,t)$ in the line-mode network can be seen as [24]:

$$\begin{cases} v_{(1)}(l,t) = v_{f(1)}\left(t - \dfrac{l}{v_{(1)}}\right) + v_{b(1)}\left(t + \dfrac{l}{v_{(1)}}\right), \\ i_{(1)}(l,t) = \left[v_{f(1)}\left(t - \dfrac{l}{v_{(1)}}\right) - v_{b(1)}\left(t + \dfrac{l}{v_{(1)}}\right)\right]/Z_{c(1)}, \end{cases} \tag{3}$$

where $v_{f(1)}$ represents the voltage of forward traveling wave (FTW), and $v_{b(1)}$ represents the voltage of backward traveling wave (BTW), $v_{(1)}$ is the velocity of line-mode TW. The direction of FTW is defined from the DC bus to the cable. In contrast, the direction of BTW is from cable to DC bus.

Since the wavefront of backward TW monitored at relay units are not refracted or reflected by the line boundaries, they are the preferred components to study the initial fault characteristics than forward traveling waves. The general BLVTW in spectral S-domain $v_{b(1)}(s)$ can be calculated as:

$$v_{b(1)}(s) = \frac{v_{(1)}(s) - Z_{c(1)}(s) i_{(1)}(s)}{2}. \tag{4}$$

To describe the attenuation effect of TWs with various fault location l, the wavefront of BLVTW $v_{b(1)12}(s)$ measured at relay unit R_{12} can be expressed as [18], [25]:

$$\begin{aligned} v_{b(1)12}(s) &= \frac{\Delta v_{F1}}{s} e^{-\Gamma(s)l} \approx \frac{\Delta v_{F1}}{s} P(s) \\ &= \frac{\Delta v_{F1}}{s}\left(\frac{1-kl}{1+s\cdot\tau l} e^{-s\cdot\frac{l}{v_{(1)}}}\right) \\ &= A_0\left(\frac{1}{s} - \frac{1}{s+1/\tau_0}\right) e^{-s\cdot T_{d0}}, \end{aligned} \tag{5}$$

where $\Gamma(s)l$ is the TW propagation coefficient representing the attenuation effect and phase shift along with l, which can be further approximated to a propagation function $P(s)$ [18]. The constant k denotes the amplitude attenuation effect per unit length, representing the real part of $\sqrt{(r_0 + j\omega L_0)(g_0 + j\omega C_0)}$. Here r_0, L_0 are the per-unit line resistance and inductance, and g_0, C_0 are the per-unit conductance and capacitance, respectively. The constant τ denotes the waveform distortion effect per unit length.

The coefficients in (5) can be calculated by:

$$A_0 = \Delta v_{F1}(1-kl), \quad \tau_0 = \tau l, \quad T_{d0} = l/v_{(1)}. \tag{6}$$

Applying the inverse Laplace transform, we obtain the expressions for the BLTVTW and the corresponding time derivative in the time-domain at relay unit R_{12} as:

$$\begin{cases} v_{b(1)12}(t) = A_0\left(1 - e^{-\frac{t-T_{d0}}{\tau_0}}\right) u\left(t - T_{d0}\right), \\ v'_{b(1)12}(t) = \dfrac{A_0}{\tau_0} e^{-\frac{t-T_{d0}}{\tau_0}} u\left(t - T_{d0}\right). \end{cases} \tag{7}$$

The expressions for $v_{b(1)21}(t)$ monitored at R_{21} can be obtained by replacing the l into $(L-l)$ in (6) and (7).

The fault location aims to estimate the fault location l in the faulty cable. According to (6) and (7), the parameter τ_0 contained in $v_{b(1)12}(t)$ is highly associated with the fault location l. Since τ is a known parameter determined by cable parameters, the fault location l can be determined by estimating the parameter τ_0 in the sampled signal $v'_{b(1)12}(t)$ using parameter fitting.

III. Proposed HVDC Fault Location Method Using AMLM-Parameter Fitting

This section introduces the principle of parameter fitting using the Adaptive Multi-step Levenberg–Marquardt (AMLM) algorithm for fault location.

A. AMLM-Based Parameter Fitting Algorithm

We consider a basic error function for parameter fitting as

$$F(A_0, \tau_0) = v'_{b(1)12} - \frac{A_0}{\tau_0} e^{-\left(\frac{t-T_{d0}}{\tau_0}\right)} = 0. \tag{8}$$

We define x as a two-dimensional matrix $x = [A_0, \tau_0]_{1\times 2}$. Then, the merit function of (8) is

$$\min_{x\in R^n} \|F(x)\|^2. \tag{9}$$

The AMLM algorithm [26] computes the trial step d_k at the k-th iteration by solving

$$\left(G_k^T G_k + \alpha_k I\right) d_k = -G_k^T F_k, \tag{10}$$

where G_k is the Jacobian. I is an identity matrix.

We define the ratio of the actual changes R_k to the predicted changes P_k of the merit function $\|F(x)\|^2$ as:

$$r_k = \frac{R_k}{P_k} = \frac{\|F_k\|^2 - \|F\left(x_k + d_k\right)\|^2}{\|F_k\|^2 - \|F_k + G_k d_k\|^2}. \tag{11}$$

The trial step x_k is updated by

$$x_{k+1} = \begin{cases} x_k + d_k, & \text{if } r_k \geq p_0, \\ x_k, & \text{otherwise}, \end{cases} \tag{12}$$

where p_0 is a small positive constant.

The Jacobian G_k is updated by

$$G_{k+1} = \begin{cases} G_k, & \text{if} \quad r_k \geq p_1 \text{ and } s < t, \\ J_{k+1}, & \text{otherwise}, \end{cases} \tag{13}$$

where $0 < p_0 < p_1 < 1$.

We update the Levenberg–Marquard parameter α_k as

$$\alpha_{k+1} = \begin{cases} \alpha_k, & \text{if } r_k \geq p_1 \text{ and } s < t, \\ \beta_{k+1}\|F_{k+1}\|^{\delta}, & \text{otherwise}, \end{cases} \tag{14}$$

where

$$\beta_{k+1}=\begin{cases}c_1\beta_k, & \text{if } r_k<p_2,\\ \beta_k, & \text{if } p_2\le r_k\le p_3,\\ \max\{c_2\beta_k,\beta_{\min}\}, & \text{if } r_k>p_3.\end{cases} \quad (15)$$

Here stands that $0<c_2<1<c_1$, $0<p_0<p_2<p_1<p_3<1$, $1\le\delta\le 2$, and $\beta_{min}>0$. Based on (10)-(15), the AMLM algorithm can be established, which can be presented as **Algorithm 1**:

Algorithm 1 The adaptive multi-step Levenberg–Marquardt algorithm

Require: $x_1\in R^n, c_1>1>c_2>0, 0<p_0<p_2<p_1<p_3<1, 1\le\delta\le 2, t\ge 1, \beta_1>\beta_{min}>0$

Ensure: Set $G_1=J_1$,$\alpha_1=\beta_1\|F_1\|^\delta$, $k:=1, s:=1, i:=1, k_i=1$

while $\left\|G_{k_i}^T F_{k_i}\right\|\neq 0$ **do**

Compute d_k by solving (10)

Compute $r_k=R_k/P_k$ by (11) and set x_{k+1} by (12)).

Update G_{k+1}, α_{k+1} and β_{k+1} by (13), (14) and (15), respectively.

Set $k=k+1$, . If G_k is the Jacobian J_k at x_k, set: $s=1, i=i+1, k_i=k$, Otherwise, set $s=s+1$.

end while

The data window used for parameter fitting starts when the TW arrives at the relay unit and ends when it is reflected at the fault point in the sampled data of $v_{b(1)12}(t)$. The parameters in **Algorithm 1** are set as: $p_0=0.0001$, $p_1=0.50$, $p_2=0.25$, $p_3=0.75$, $c_1=4$, $c_2=0.25$, $\beta_1=10^{-5}$, $\beta_{min}=10^{-8}$, and $t=10$. The values for k and τ in (6) are set to $k=5.0\times10^{-5}$/km and $\tau=1.5\times10^{-8}$s/km to achieve the optimal parameter fitting results after numerous simulation tests.

B. Proposed Single-ended Fault Location Method

The coefficients A_0 and τ_0 can be obtained according to the optimal solution of x_k generated by **Algorithm 1**. Then, the estimated fault location l^* can be determined as:

$$l^*=\frac{\tau_0}{\tau}. \quad (16)$$

The proposed AMLM-based fault location method can be illustrated in Fig. 3:

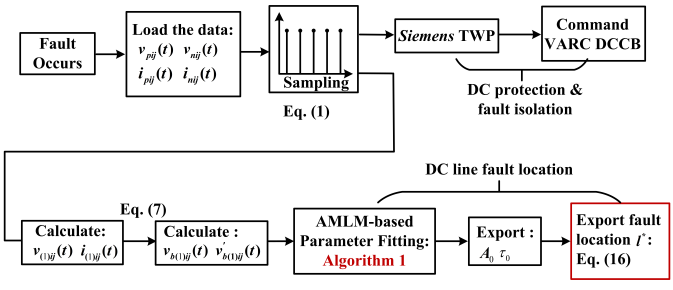

Fig. 3. Illustration of the proposed fault location method.

IV. Experimental Simulation Results

A. RTDS Set-up

RTDS is utilized for simulating the model depicted in Fig. 1. MMC1 to MMMC3 are all modeled using the valve model $'rtds\_vsc\_FPGA\_GM'$ in RSCAD/RTDS. The MMCs' capacitor voltage balancing and firing pulse control are realized using the Xilinx Virtex-7 FPGA board (GTFPGA) for its high computation ability [27]. An interface transformer connects the small time step subsystem to the main system with a large time step, which allows using a 2 μs solution-time step for VARC DCCB and MMCs components. The other system components adopt a 50 μs main solution step. In addition, two NovaCor racks are used to model the testing system. The cross-rack communication is conducted via a global bus hub and an IRC switch [27]. The signal exchanges between GTFPGA units and RTDS NovaCor racks are performed via fiber optic cables with the IEC 61850-9-2 standard.

B. Fault Location Results

To validate the proposed DC fault location method, the internal fault f_{12} described in Section II is applied at $t=0.2$ s. The fault resistance R_f is set as 0.001 Ω and 1.0 Ω as the cable faults are mostly metallic or small-impedance faults in reality [28]. The TWs data in RTDS is sampled with a sampling frequency of 20 kHz. The AMLM-based fault location algorithm is coded in Matlab to analyze the data collected from RTDS platform.

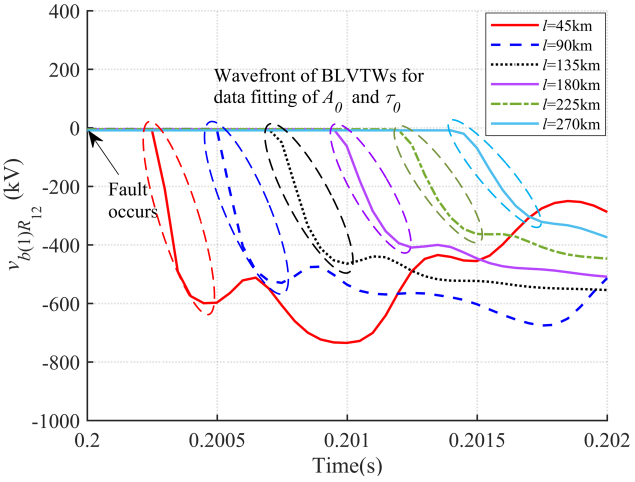

Fig. 4. Monitored $v_{b(1)12}(t)$ at relay R_{12} with different fault distance l.

The results of $v_{b(1)12}(t)$ under PTP fault is shown in Fig. 4. In the steady-state, the amplitude of $v_{b(1)12}(t)$ is zero. After DC fault occurrence, the fault-induced voltage Δv_{F1} propagates along the faulty cable, as described in (5). The wavefront of BLTVTW $v_{b(1)12}(t)$ approximates to an exponential function as expressed with equation (7). Its arriving time and attenuation level are related to the fault location l.

TABLE II
FAULT LOCATION RESULTS

l	R_f=0.001 Ω Fault type	l^*	Error (%)	l	R_f=1.0 Ω Fault type	l^*	Error (%)
45km	PTG	45.37	0.12	45km	PTG	46.16	0.39
	NTG	45.41	0.14		NTG	44.63	0.12
	PTP	45.84	0.28		PTP	46.40	0.47
90km	PTG	89.40	0.20	90km	PTG	89.62	0.12
	NTG	89.41	0.19		NTG	89.60	0.13
	PTP	88.96	0.34		PTP	88.57	0.47
135km	PTG	134.14	0.28	135km	PTG	134.24	0.25
	NTG	135.13	0.05		NTG	134.23	0.25
	PTP	133.89	0.36		PTP	133.94	0.35
180km	PTG	179.51	0.16	180km	PTG	178.99	0.33
	NTG	179.40	0.19		NTG	179.10	0.29
	PTP	179.16	0.28		PTP	178.52	0.49
225km	PTG	226.05	0.35	225km	PTG	224.46	0.17
	NTG	226.00	0.33		NTG	224.48	0.17
	PTP	224.39	0.20		PTP	223.80	0.40
270km	PTG	270.50	0.16	270km	PTG	271.01	0.33
	NTG	270.61	0.20		NTG	270.93	0.30
	PTP	271.23	0.41		PTP	271.75	0.58

TABLE III
FAULT LOCATION RESULTS WITH 40DB NOISE

l	R_f=0.001 Ω Fault type	l^*	Error (%)	l	R_f=1.0 Ω Fault type	l^*	Error (%)
45km	PTG	46.92	0.64	45km	PTG	47.21	0.74
	NTG	46.09	0.36		NTG	46.42	0.47
	PTP	46.27	0.42		PTP	47.35	0.78
90km	PTG	88.47	0.51	90km	PTG	89.75	0.08
	NTG	88.36	0.54		NTG	88.74	0.41
	PTP	87.73	0.75		PTP	88.97	0.34
135km	PTG	132.41	0.86	135km	PTG	134.48	0.17
	NTG	136.56	0.52		NTG	133.15	0.61
	PTP	133.05	0.65		PTP	134.74	0.09
180km	PTG	178.04	0.65	180km	PTG	178.66	0.44
	NTG	178.23	0.59		NTG	178.21	0.59
	PTP	177.83	0.72		PTP	178.05	0.64
225km	PTG	227.17	0.72	225km	PTG	225.60	0.20
	NTG	226.89	0.63		NTG	223.98	0.33
	PTP	226.87	0.62		PTP	222.98	0.67
270km	PTG	271.97	0.66	270km	PTG	272.77	0.92
	NTG	268.84	0.38		NTG	271.46	0.49
	PTP	272.23	0.74		PTP	272.88	0.95

The estimation error to evaluate the accuracy of the proposed fault location method can be seen as follows:

$$\text{Error} = \left| \frac{l - l^*}{L_{cable12}} \right| \% \tag{17}$$

where $L_{cable12}$ is 300km.

The fault location results are summarized in Table II. The results are accurate as all the estimated errors are smaller than 1%. The most serious case is the $f_{12}|(\text{PTP}, x = 270\text{km}, R_f = 1\Omega)$, where the estimated fault distance $l^* = 271.75$ km, and the largest difference with the real fault distance is 1.75 km. Besides, it is visible that fault resistance R_f and the fault type do not significantly impact the accuracy since the R_f and fault type only affect the initial value of Δv_{F1}, as it is visible from equations (2) and (6). They will not impact the parameters A_0 and τ_0 of the exponential function $v'_{b(1)12}(t)$. Thus, it is concluded that the R_f and fault type will not affect the accuracy of the parameter fitting process.

C. Noise Test

In practical HVDC engineering, the presence of noise can have a significant impact on the performance of protection and fault location algorithms. To validate the performance of the proposed method under noise interference, Gaussian white noise (GWN) is added to the sampled TW data with a signal-to-noise ratio (SNR) level of 40 dB.

According to the results in Table. III, it is apparent that the GWN reduces the accuracy compared with the results in Table. II. This is due to the reason that the object of parameter fitting is the time derivative of $v'_{b12(1)}(t)$, of which the calculation of the derivative is susceptible to noise. The most serious case is $f_{12}|(\text{PTP}, x = 270\text{km}, R_f = 1.0\Omega)$, the largest error with the real fault distance is 2.88 km. Overall, the fault location results under noise interference are accurate as all the estimated errors are smaller than 1%. Therefore, the results confirm that the proposed method is sufficiently robust and accurate to withstand noise interference.

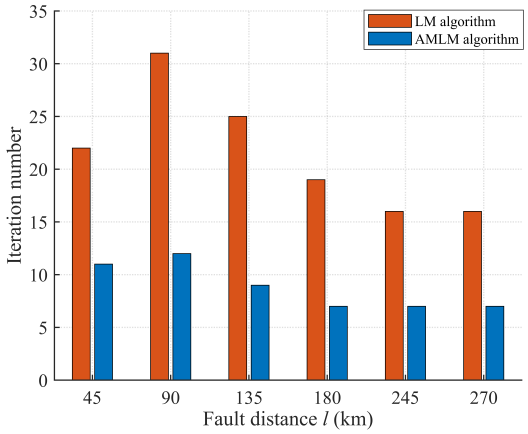

Fig. 5. Comparison of iteration numbers for parameter fitting between AMLM and LM algorithm in [29].

D. Comparison Study

Although the classical parameter fitting method in [29] has better computational accuracy than the other algorithms, such as the Gradient Descent algorithm, Newton's algorithm, Gaussian Newton's algorithm, etc., it has a long computation time. It requires large memory due to massive iterations for Jacobi matrix. The AMLM algorithm used in our work can solve this problem efficiently. The comparison results are shown in Fig. 5. The iteration number of AMLM algorithm is

much less than that of the location method presented in [29] when fitting the parameters of sampled TW data, effectively reducing computation time and memory size while ensuring fault location accuracy.

V. Conclusion

This study presents a fresh perspective on the fault location method for the MTDC system using backward line-mode voltage TWs. First, it is shown that the wavefront of backward line-mode voltage TWs can be approximated to an exponential function, with the DC fault distance embedded in its parameter. Next, the AMLM algorithm is utilized as the parameter fitting tool, offering high accuracy and iteration speed. The calculating procedure of the AMLM algorithm is also explained in detail. Lastly, the accuracy of the fault location method is validated via RTDS platform.

Based on the results, the proposed method is accurate, with all the errors being less than 1%. Furthermore, its performance is independent of fault resistance and type. The proposed method does not require a high sampling frequency and communication channel, thus significantly reducing the hardware requirements and investment in practical applications. The authors also thoroughly investigated noise tests. The presented results confirm the superior performance in withstanding the 40 dB noise. However, further efforts are still needed to improve the method in withstanding noise interference and fault location accuracy.

References

[1] A. Shetgaonkar, L. Liu, A. Lekić, M. Popov, and P. Palensky, "Model predictive control and protection of mmc-based mtdc power systems," *International Journal of Electrical Power & Energy Systems*, vol. 146, p. 108710, 2023.

[2] A. Heidary, M. Popov, A. Moghim, M. G. Niasar, and A. Lekić, "The principles of controlled dc reactor fault current limiter for battery energy storage protection," *IEEE Transactions on Industrial Electronics*, pp. 1–9, 2023.

[3] Z.-Y. He, K. Liao, X.-P. Li, S. Lin, J.-W. Yang, and R.-K. Mai, "Natural frequency-based line fault location in hvdc lines," *IEEE transactions on power delivery*, vol. 29, no. 2, pp. 851–859, 2013.

[4] G. Song, X. Chu, X. Cai, S. Gao, and M. Ran, "A fault-location method for vsc-hvdc transmission lines based on natural frequency of current," *International Journal of Electrical Power & Energy Systems*, vol. 63, pp. 347–352, 2014.

[5] J. He, B. Li, Q. Sun, Y. Li, H. Lyu, W. Wang, and Z. Xie, "The improved fault location method based on natural frequency in mmc-hvdc grid by combining fft and music algorithms," *International Journal of Electrical Power & Energy Systems*, vol. 137, p. 107816, 2022.

[6] N. Bayati, H. R. Baghaee, A. Hajizadeh, M. Soltani, Z. Lin, and M. Savaghebi, "Local fault location in meshed dc microgrids based on parameter estimation technique," *IEEE Systems Journal*, vol. 16, no. 1, pp. 1606–1615, 2021.

[7] D. Li and A. Ukil, "Fault location estimation in voltage source converter based dc system: The l location," *IEEE Transactions on Industrial Electronics*, 2021.

[8] J. Xu, Y. Lü, C. Zhao, and J. Liang, "A model-based dc fault location scheme for multi-terminal mmc-hvdc systems using a simplified transmission line representation," *IEEE Transactions on Power Delivery*, vol. 35, no. 1, pp. 386–395, 2020.

[9] S. Jiang, C. Fan, N. Huang, Y. Zhu, and M. He, "A fault location method for dc lines connected with dab terminal in power electronic transformer," *IEEE Transactions on Power Delivery*, vol. 34, no. 1, pp. 301–311, 2018.

[10] T. Roose, A. Lekić, M. M. Alam, and J. Beerten, "Stability analysis of high-frequency interactions between a converter and hvdc grid resonances," *IEEE Transactions on Power Delivery*, vol. 36, no. 6, pp. 3414–3425, 2021.

[11] G. Song, J. Hou, B. Guo, T. Wang, B. Masood, and S. T. H. Kazmi, "Single-ended active injection for fault location in hybrid mmc-hvdc systems," *International Journal of Electrical Power & Energy Systems*, vol. 124, p. 106344, 2021.

[12] T. Bi, S. Wang, and K. Jia, "Single pole-to-ground fault location method for mmc-hvdc system using active pulse," *IET Generation, Transmission & Distribution*, vol. 12, no. 2, pp. 272–278, 2018.

[13] T. Wang, G. Song, and K. S. T. Hussain, "Adaptive single-pole auto-reclosing scheme for hybrid mmc-hvdc systems," *IEEE Transactions on power delivery*, vol. 34, no. 6, pp. 2194–2203, 2019.

[14] L. Yuansheng, W. Gang, and L. Haifeng, "Time-domain fault-location method on hvdc transmission lines under unsynchronized two-end measurement and uncertain line parameters," *IEEE Transactions on Power delivery*, vol. 30, no. 3, pp. 1031–1038, 2015.

[15] S. Lan, M.-J. Chen, and D.-Y. Chen, "A novel hvdc double-terminal non-synchronous fault location method based on convolutional neural network," *IEEE Transactions on Power Delivery*, vol. 34, no. 3, pp. 848–857, 2019.

[16] C. Zhang, G. Song, T. Wang, and L. Yang, "Single-ended traveling wave fault location method in dc transmission line based on wave front information," *IEEE Transactions on Power Delivery*, vol. 34, no. 5, pp. 2028–2038, 2019.

[17] Y. Wei, P. Sun, Z. Song, P. Wang, Z. Zeng, and X. Wang, "Fault location of vsc based dc distribution network based on traveling wave differential current with hausdorff distance and cubic spline interpolation," *IEEE Access*, vol. 9, pp. 31 246–31 255, 2021.

[18] S. Yang, W. Xiang, and J. Wen, "An improved dc fault protection scheme independent of boundary components for mmc based hvdc grids," *IEEE Transactions on Power Delivery*, vol. 36, no. 4, pp. 2520–2531, 2020.

[19] W. G. Cigré, "B4. 57."Guide for the Development of Models for HVDC Converters in a HVDC Grid"," *CIGRE Technical Brochure*, vol. 604, 2014.

[20] C. Zhang, G. Song, T. Wang, and X. Dong, "An improved non-unit traveling wave protection method with adaptive threshold value and its application in hvdc grids," *IEEE Transactions on Power Delivery*, vol. 35, no. 4, pp. 1800–1811, 2020.

[21] S. Liu, M. Popov, S. S. Mirhosseini, S. Nee, T. Modeer, L. Ängquist, N. Belda, K. Koreman, and M. A. M. M. van der Meijden, "Modeling, experimental validation, and application of varc hvdc circuit breakers," *IEEE Transactions on Power Delivery*, vol. 35, no. 3, pp. 1515–1526, 2020.

[22] L. Liu, A. Lekić, and M. Popov, "Robust traveling wave-based protection scheme for multiterminal dc grids," *IEEE Transactions on Power Delivery*, pp. 1–13, 2023.

[23] S. S. Mirhosseini, S. Jamali, and M. Popov, "Non-unit protection method for long transmission lines in mtdc grids," *IET Generation, Transmission & Distribution*, vol. 15, no. 11, pp. 1674–1687, 2021.

[24] L. Tang, X. Dong, S. Shi, and B. Wang, "Analysis of the characteristics of fault-induced travelling waves in mmc-hvdc grid," *The Journal of Engineering*, vol. 2018, no. 15, pp. 1349–1353, 2018.

[25] C. Zhang, G. Song, T. Wang, L. Wu, and L. Yang, "Non-unit traveling wave protection of hvdc grids using levenberg–marquart optimal approximation," *IEEE Transactions on Power Delivery*, vol. 35, no. 5, pp. 2260–2271, 2020.

[26] J. Fan, J. Huang, and J. Pan, "An adaptive multi-step levenberg–marquardt method," *Journal of Scientific Computing*, vol. 78, no. 1, pp. 531–548, 2019.

[27] L. Liu, A. Shetgaonkar, and A. Lekić, "Interoperability of classical and advanced controllers in mmc based mtdc power system," *International Journal of Electrical Power & Energy Systems*, vol. 148, p. 108980, 2023.

[28] L. Liu, Z. Liu, M. Popov, P. Palensky, and M. A. M. M. van der Meijden, "A fast protection of multi-terminal hvdc system based on transient signal detection," *IEEE Transactions on Power Delivery*, vol. 36, no. 1, pp. 43–51, 2021.

[29] C. Zhang, Y. Li, G. Song, and X. Dong, "Fast and sensitive nonunit protection method for hvdc grids using levenberg–marquardt algorithm," *IEEE Transactions on Industrial Electronics*, vol. 69, no. 9, pp. 9064–9074, 2021.